



Chitosan/Polyvinyle Alcohol with Silver Nanoparticles for Antimicrobial Applications

A. M. Hezma^{1*}, A. M. Abdelghany¹, M. S. Abdel-Aziz² and I. S. Elashmawi^{1,3}

¹Spectroscopy Department, Physics Division, National Research Centre, Dokki, 12311, Giza, Egypt

²Microbial Chemistry Department, Genetic Engineering and Biotechnology Division, National Research Centre, Dokki, 12311, Giza, Egypt

³Physics Department, Faculty of Science at Al-Ula, Taibah University, Saudia Arabia

ABSTRACT

An in-situ preparation technique was used for preparation of equimass samples (chitosan/poly vinyl alcohol, CS/PVA) embedded with silver nanoparticles (AgNPs). X-ray diffraction scans (XRD) showed the appearance of two new peaks with increasing silver content. XRD showed that the intensity of the peak $2\theta = 18.6^\circ$ slightly decreased after adding AgNPs indicating that strong interaction occurred between PVA and CS and an increase in the amorphous phase in the polymeric matrices. Fourier transform infrared spectra (FTIR) showed the main characteristic bands corresponding to the polymeric constituents (CS/PVA). The UV/vis. absorption spectra and XRD scans revealed the presence of the semi-crystalline nature of the polymeric composites. The obtained polymer nano-composites were also examined for their antibacterial effect against Gram +Ve, Gram -Ve and spore forming bacteria. The nano-composite samples showed better film properties than that of the pristine polymer blends without silver nanoparticles.

Keywords: Chitosan/poly vinyl alcohol (CS/PVA); AgNPs; SEM; FTIR; antimicrobial activities.

INTRODUCTION

Chemical reduction technique comprises one of the most common reported methods for developing silver nanoparticles (AgNP). Reduction method that uses chemicals including hydrazine hydrate, ethylene glycol, dimethyl formamide and other available chemicals may cause toxicity and/or biological hazards [1-3]. Recent trends in nanotechnology research involving use of eco-friendly polymers that can achieve stabilization as well as reduction during synthesis process of silver nanoparticles [1]

Water soluble biopolymers in combination with AgNP were expected to produce new antimicrobial activities. A stream of natural polymers have been employed for the preparation process of polymeric AgNP nanocomposites [2, 3]. Chitosan (CS) is a natural biocompatible biopolymer which degraded within human body by enzymes without further cytotoxicity [4]. Adsorption efficiency for water can be related to their crystalline nature [5]. Chitosan displays a broad spectrum of antimicrobial activities due to their mechanism of binding to the negatively charged cell wall of bacteria followed by their connection to DNA which leads to inhibiting its replication [6, 7]. Bioactivity of chitosan could be improved by its combination with other bioactive materials such as drugs. Chitosan interacts very easily with bacterial DNA, glycosaminoglycan and most bacterial proteins, thereby enhancing the antibacterial properties [7].

Polyvinyl alcohol (PVA) represent a nontoxic, synthetic and water soluble polymer used in stabilization in nanoparticles synthesis [8-10] and their blend with chitosan exhibits antimicrobial activity against pathogenic bacteria in food packaging preparation [11]. Films and coatings based on biopolymer (i.e., chitosan, cellulose, etc.)

have been proposed to function as blocks towards moisture, oil as well as aroma flavor, they can be called a materials for future applications [12]. Furthermore, polymeric thin film doped with silver nanoparticles showed an antimicrobial activity up to 99.99% against *Escherichia coli* and *Staphylococcus aureus*, so that it could be used as an antimicrobial wound-dressing material for chronic wounds and burns [13, 14]. Materials that contains silver and/or silver ion are used as catheters, vascular grafts, prostheses and as wound dressings [15, 16]. Recently, authors shows that silver nanoparticles is much more effective bulk silver or silver ions as an antimicrobial [17, 18]. Antimicrobials silver nanoparticles are environmentally and health safe in addition to their high thermal stability [19]. Commercial silver containing products such as augmentation devices, bandages, topical ointments, tissue scaffolds, antimicrobial gels and filters were used in the last decade for improving public health care [20, 21]. Different authors discovered that silver possess an ability for treatment of cancer [22]. Silver is not specific at targeting cancer cells and it has been found that it is toxic for normal cells to get exposed to silver nanoparticles of size > 20 nm for long time [23-25].

Inorganic nanoparticles that have antimicrobial activities can be classified as a new class of biomedical materials that satisfies the increasing demands for hygiene in our daily life. In particular, copper or silver nanoparticles were extensively used in many bactericidal fields [26]. Their major antimicrobial activities can be related to their strong cytotoxicity for different bacterial cells [27]. Recently, polymeric matrices have been examined as protective mediators to stabilize AgNPs and avoid their aggregation [28]. This work was undertaken with the objective of synthesizing CS/PVA–Ag nanocomposite by a chemical method with different concentrations of silver. Different spectroscopic techniques were used for sample characterization including (FTIR) Fourier transform infrared, electronic UV/vis. and X-ray diffraction analysis (XRD). The antimicrobial activities against different tested microbes were also studied.

MATERIALS AND METHODS

2.1. Sample preparation and measurement techniques

The basic materials used in this study include polyvinyl alcohol ((PVA) (C₂H₄O)_n of M_w= 14000 gm/mol), chitosan (CS) (low molecular weight (75-85% deacetylated)) and silver nitrate (AgNO₃), all supplied by Sigma-Aldrich Co. (USA).

Films of AgNPs/PVA/CS were synthesized using solution casting method as in the following steps. Solutions of equal weights of PVA and CS were prepared using double distilled water with constant stirring at 60°C. Gradient concentrations of AgNO₃ was added to the PVA/CS poly blend solutions continuously stirred at 60°C for about 3 hours to ensure their homogeneity as indicated in table 1. Homogeneous solution was casted into Petri dishes and left to dry at 50°C for 3 days to form the desired film with a thickness from about 0.5 mm to 1.0 mm, and then the films were stripped off the dish. X-ray diffraction scans were performed using a PAN analytical X' Pert PRO XRD system (Holland) in reflection or transmission region, using Cu-K_α target radiation (where λ=1.540 Å, and tube operating at 45 kV-40 mA). All samples were measured in Bragg angle (2θ) range of 5-60°. FT-IR absorption spectra were measured for different films using a single beam Fourier transform-infrared spectrometer (Nicolet iS10, USA) at room temperature in the spectral range of 4000–400 cm⁻¹. UV-visible absorption spectra were measured in the wavelength region of 190-1100 nm using aV-570 UV-VIS-NIR spectrophotometer (JASCO, Japan). Transmission electron microscopy (TEM) studies were done of nanoparticle films formed on carbon coated copper grids (40 μm × 40 μm mesh size), using a JEOL 1200 EX (Japan) transmission electron microscope, operating at an accelerated voltage of 120 kV.

Table (1) Sample composition and notation

Sample notation	PVA	CS	AgNO ₃
	Wt%		
S0	50	50	0.00
S1	49.95	49.95	0.10
S2	49.90	49.90	0.20
S3	49.80	49.80	0.40
S4	49.60	49.60	0.80

Agar plate method has been established to evaluate the antimicrobial activities of prepared samples that contains AgNPs compared with a positive control (PVA) and pure blend films (PVA/CS) according to the Collins and Lyne method [29, 30]. Four different test microbes; *Staphylococcus aureus*, *Escherichia coli*, *Candida albicans* and *Aspergillus niger* were selected to evaluate the antimicrobial activities as representatives of G+ve bacteria, G-ve bacteria, yeast and fungal groups. The bacterial and yeast test microbes were grown on a nutrient agar medium. On the other hand, the fungal test microbe was cultivated on Czapek-Dox medium. The culture of each test microbe was diluted by distilled water (sterilized) to 10⁷ to 10⁸ colony forming units (CFU)/ml then 1ml of each was used to inoculate 1L-Erlenmeyer flask containing 250ml of solidified agar media. These media were put onto previously sterilized Petri dishes (10 cm diameter having 25ml of solidified media).

The discs (15 mm) from the different polymer specimens (PVA, PVA/CS and PVA/CS/Ag) were placed onto the inoculated agar plate surfaces and incubated for 24h at 37°C (bacteria). But the fungus was incubated for 48h at 30°C. On the other hand, yeast was incubated for 24h at 30°C. Antimicrobial activities were recorded as the diameter of the clear zones (including the film itself) that appeared around the films.

The antibacterial of PVA, PVA/CS and PVA/CS/Ag blends were also investigated using a plate count technique by measuring the colony forming unit (CFU) method. *S. aureus* stock culture was used to cultivate nutrient broth medium and incubated at 37 °C for 24h. Samples were supplied to the bacterial-cultivated flasks. A control sample was constructed (without any specimens). After 16h incubation at 37 °C, a serial dilution from each sample-containing culture and the control has been done (10^{-2} - 10^{-7}). The reduction in the bacterial was monitored by two ways. In the first, the solidified nutrient agar in Petri dishes were inoculated by 100 μ l from each dilution and the CFU was detected and the loss in the growth rate (R) for culture flasks containing polymers samples against to the culture media without any samples were detected according to the following Eq.[31]:

$$R (\%) = \frac{B-A}{B} \times 100$$

Where: A is colony forming units for the culture treated samples (S1-S4) after 16-h incubation and B is colony forming units for the culture untreated sample (S0) under the same incubation conditions [32]. In the next way, the optical density of the incubated nutrient broth medium was detected at 660 nm against control culture of *S. aureus*. The optical density was directly proportional to the increment in the number of the bacteria in the medium.

2.2. Calculation of the nanoparticle size

One of the most characteristic features of the nanoparticle is the size despite their shape and distribution because it can control the main characteristic features of the prepared nanoparticles. Many methods can be used for particle size determination including direct experimental methods such as TEM and dynamic light scattering (DLS) in addition to information which can be obtained from indirect experimental methods such as XRD using well-known Scherrer formula [1, 25]:

$$L = K\lambda/\beta \cos(\theta)$$

Where L is the average crystallite size, λ is the X-ray wavelength in nanometer (nm), β is the peak width at half maximum of the diffraction peak in radians and K is a shape factor related to crystallite shape, normally 0.9. Mie theory applies classical electrodynamics to cluster of simple shapes like spheres introduce a precise indirect experimental method captured from the UV/vis. measurements.

RESULTS AND DISCUSSION

3.1. X-ray diffraction analysis

Figure 1 shows X-ray diffraction (XRD) scans for PVA/CS with 0, 0.1, 0.2, 0.4 and 0.8 wt.% of AgNPs. The pure PVA/CS film (S0) showed the characteristic pattern of an amorphous phase with the main halo of the typical broad peak at a 2θ of 18.6°, a shoulder at a 2θ of 22.5°[33] and another broad peak at 41.2°. The X-ray diffraction pattern for S1, S2, S3 and S4 films show the peaks of PVA/CS and several sharp diffraction peaks at $2\theta = 32^\circ$ and 46° . These peaks are assigned to the face-centred-cubic (fcc) structure of the embedded Ag metal nanoparticles corresponding to the $h k l$ parameters (111) and (200) which increase in intensity with increasing Ag content. Observed bands were compared with the standard powder diffraction card of Joint Committee on Powder Diffraction Standards (JCPDS), No. 04-0783. Presence of a large number of self-agglomerated nanoparticles in sample (S4) of high level of AgNPs leads to increase in crystalline character of the nanocomposite. Diffraction pattern also indicates all films consists of two phase structure (amorphous polymer and nanoparticles) based on absence of a new peak or a peak shift compared with the pure PVA/CS. This remark proves that addition of AgNPs causes no change in the crystallinity of PVA/CS polymer blend.

3.2. FT-IR analysis

The FT-IR spectra of CS/PVA filled with various fractions of AgNPs in the spectral range of 4000-400 cm^{-1} is shown in Fig. 2. The absorption peak observed at 3400 cm^{-1} attributed to OH/NH₂ indicates the presence of hydrogen bonds [34]. From the FT-IR spectra of the pure PVA/CS film (S0) the bands around 1632, 1325 and 1550 cm^{-1} were assigned to amide I (C=O), amide II (-NH) and asymmetric stretching mode of -CH₂ group of the organic matrix, respectively. The peak observed at 2920 cm^{-1} is characteristic of -CH₂ asymmetric stretching of CS/PVA. The CS/PVA films loaded with silver nanoparticles (Fig. 2 (S2-S4)) showed all the above characteristic peaks with a slight shift and large decreasing intensity of the peak 1550 to 1511 cm^{-1} corresponding - CH₂ asymmetric stretching

band. There were decreases also in intensity of other bands, including 2920, 1746 and 1240 cm^{-1} , showing that AgNPs were bound to functional groups that present in both chitosan and PVA. The increase of intensity of NH peak may be attributed to co-ordination bond formation between electron rich groups (oxygen/ $-\text{NH}$) present in chitosan to silver which results in change in bond length and/or frequency. These mentioned observations confirm presence of silver nanoparticles in the chitosan-PVA film networks.

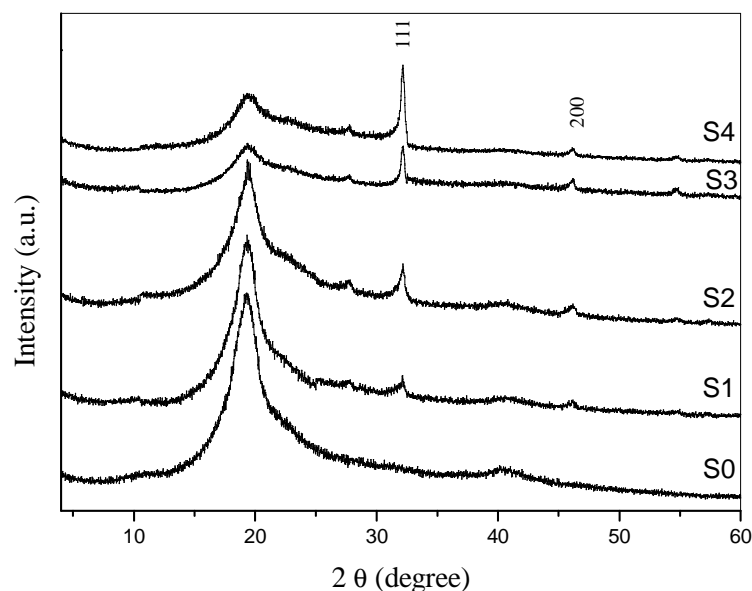


Fig. 1: X-ray diffraction (XRD) scans for the PVA/CS blend and the blend with various AgNPs contents

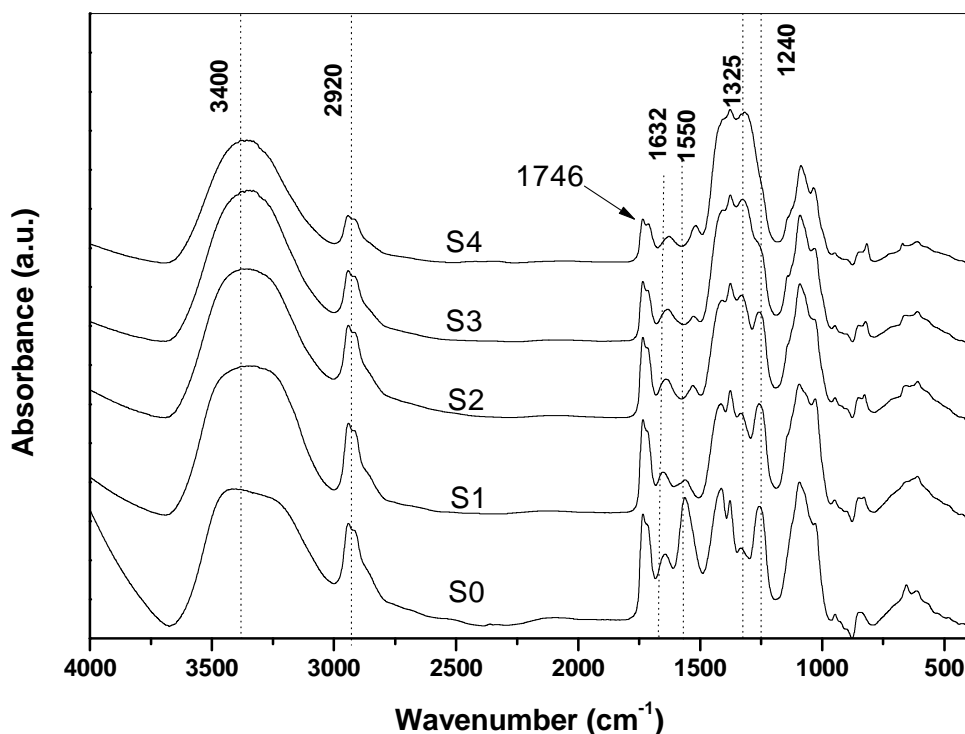


Fig. 2: FTIR absorption spectra for peaks PVA/CS blends and the blends with various AgNPs contents

3.3. UV/vis. optical absorption spectra

Figure 3 shows the UV/vis. absorption spectra in the wavelength range of 200-1100 nm for all doped samples at room temperature. A sharp peak at 246 nm for pure blend which attributed to $\pi \rightarrow \pi^*$ transitions was observed. The peak comes from unsaturated bonds ($\text{C}=\text{O}$ and/or $\text{C}=\text{C}$). The characteristic band at around 438 nm for 0.2 wt.% of AgNP (S1) is attributed to of AgNPs (S1). The intensity of this band increases with increase of the Ag nanoparticles.

The shift of this band to lower wavelength (as shown in 3) indicates a decrease of grain sizes of the Ag nanoparticles within the blend with higher the content for 0.8 wt.% of AgNPs (S4). Furthermore, the absorption band at 298 nm, associated with the NO₃ compound, increases with increasing AgNPs. Moreover, all curves are characterized by the presence of an exponential decay tail at high wavelength, indicating the presence of localized states in the energy band gap.

The optical energy band gap (distance between HUMO and LUMO) was determined from the plot of photon energy ($h\nu$) versus $(\alpha h\nu)^{1/n}$, where α is the absorption coefficient and n characterizes the type of transition, n has values, 1/2, 2, 3/2 and 3 for direct, indirect, forbidden direct and forbidden indirect transitions, respectively. The relation between the photon energy ($h\nu$) versus $(\alpha h\nu)^{1/2}$ was plotted as shown in Fig. 4 and used to calculate to optical gap. Assessment of the optical absorption spectra measurement at 448 nm was done using Mott and Davis formula for direct optical band. The band gap energies were determined from the extrapolation of the linear section of the curves to the x-axis for which $(\alpha h\nu)^2 = 0$ [35]. The band gap energies at various dopant concentrations AgNPs are shown in Fig. 4. A blue shift to 418 nm was observed for highest concentration of AgNPs compared with that of bulk Ag at 510 nm, suggesting the formation of nanometer-sized particles of Ag which is in an agreement with the XRD results.

The calculated values of the energies band gap decreased with increasing of AgNPs concentration which was explain on the basis of the fact that the incorporation of a small amount of dopant forms charge transfer complexes in the host lattice (polymer blend) and Ag⁺ ions. This results in the formation of defects in polymeric matrix. These defects produce localized states in the optical band gap. They are responsible for decreasing the band gap energy when the Ag-filler was increased in the polymeric matrix.

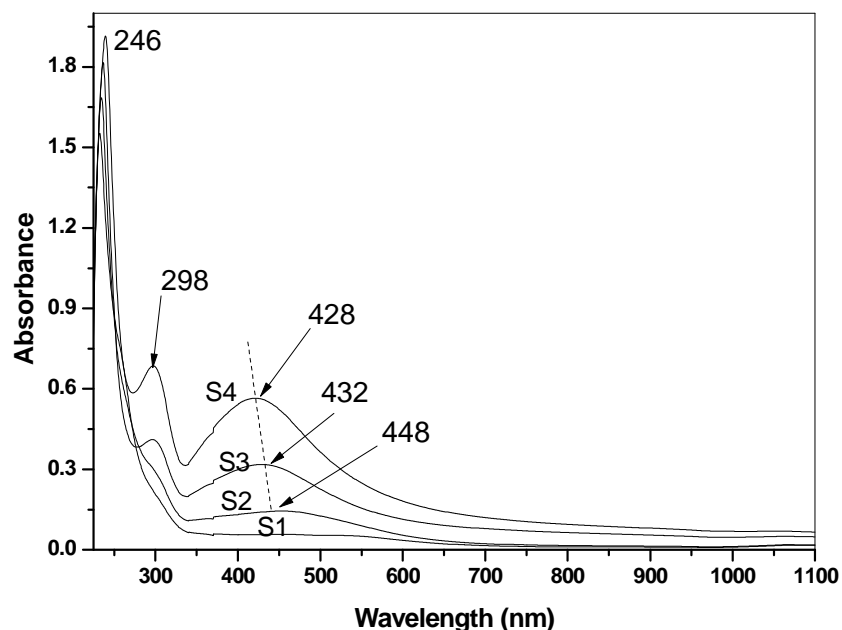


Fig. 3: UV/vis. absorption spectra for the PVA/CS blends with various AgNPs contents

3.4. TEM analysis

Fig. 5 depicts TEM images of the morphology, distribution of silver nanoparticles dispersed within Cs/PVA polymer blend. Image (S1) is of the nanocomposite films with 0.2 wt.% of silver nanoparticles. The single particles have sizes in the range of 20 ± 2 nm. When the amount of Ag nanoparticles increased to 0.4 wt.% (S2), the sizes of the particles were decreased to the range $\approx 16 \pm 2$ nm and at the amount of 0.8 wt.% of silver (S3), the aggregation of silver nanoparticles appeared with individual particle size, in the range 8 ± 2 nm. As shown in these images higher number of the particles were clearly in spherical shapes which were connected together and network in some areas rich in silver clusters uniformly distributed within the polymeric matrix. Obtained data was in agreement with that obtained from UV/vis. optical absorption spectra using Mie theory and from X-ray diffraction using Scherrer formula.

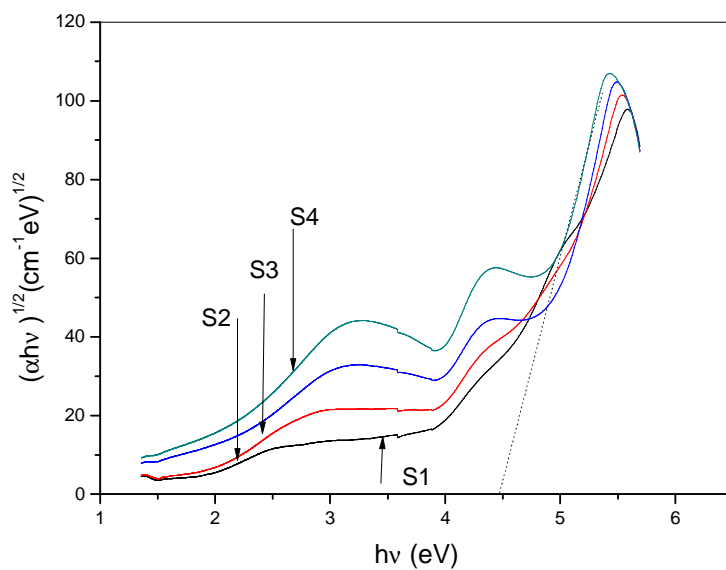
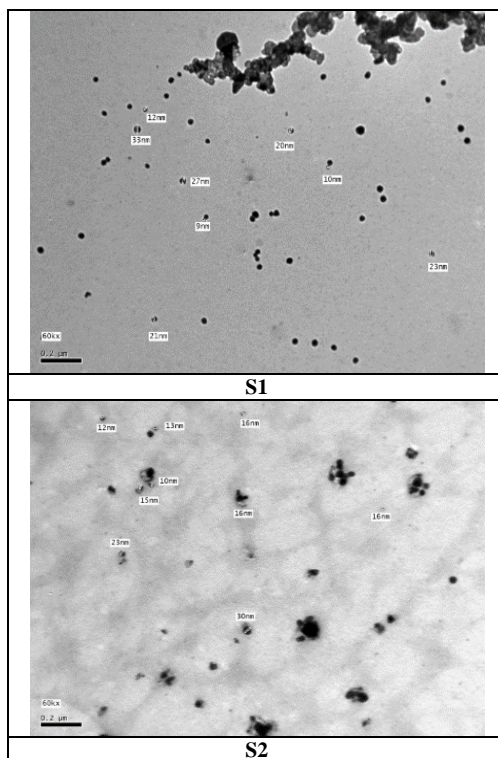


Fig.4: The relation between the photon energy(hv) various $(\alpha hv)^{1/2}$

It is clear from the images that the average size was decreased with increasing the amount of Ag. From the UV/vis. spectra, X-ray diffraction and TEM images; it was found that a higher amount of silver resulted in a smaller size with a good dispersing within polymeric matrix.



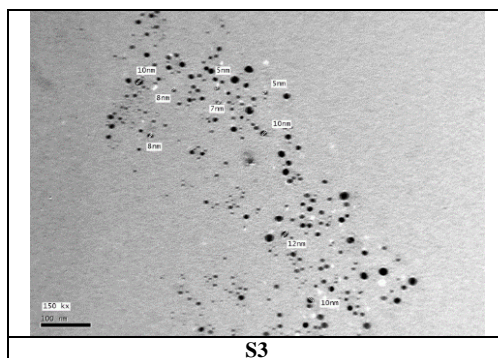


Fig.5: TEM images of the morphology, distribution of silver nanoparticles dispersed within Cs/PVA polymer blend

3.5. Antimicrobial test

The results in Table 2 and Fig. 6 indicate that PVA and the PVA/CS blend didn't exhibit any antimicrobial activity, whereas samples S1, S2, S3 and S4 showed antimicrobial activity against the test microbes. The activity increased from S1 to S4 with maximum activity for S4 which give a clear zone of 25 mm (including the film diameter) against *Staphylococcus aureus*, 23 mm with *E. coli*, 25mm with *Candida albicans* and 45mm with *Aspergillus niger*.

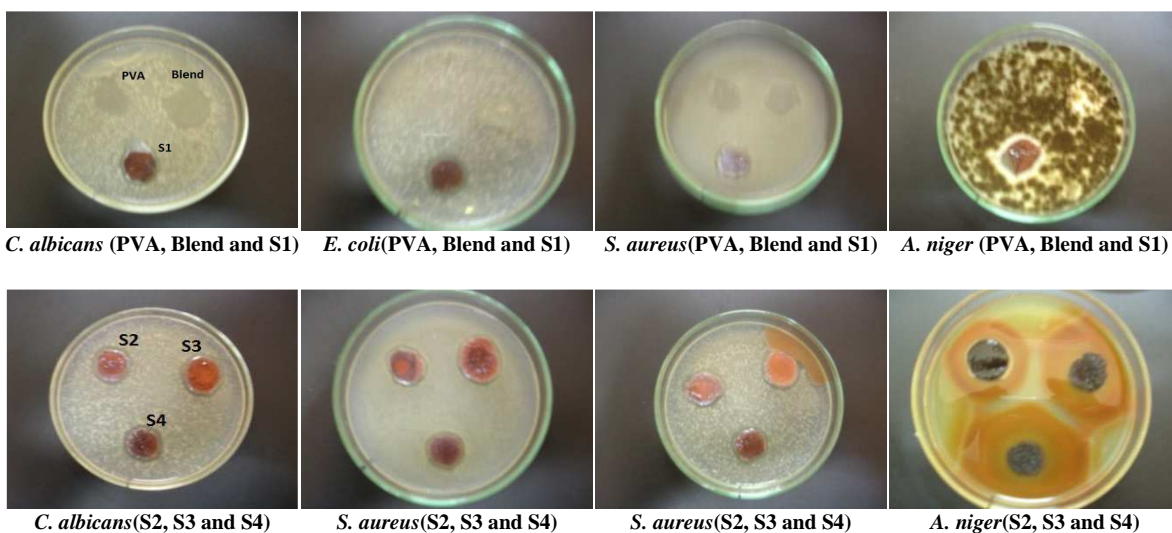


Fig.6: The antimicrobial activity of different samples using the disk agar diffusion method

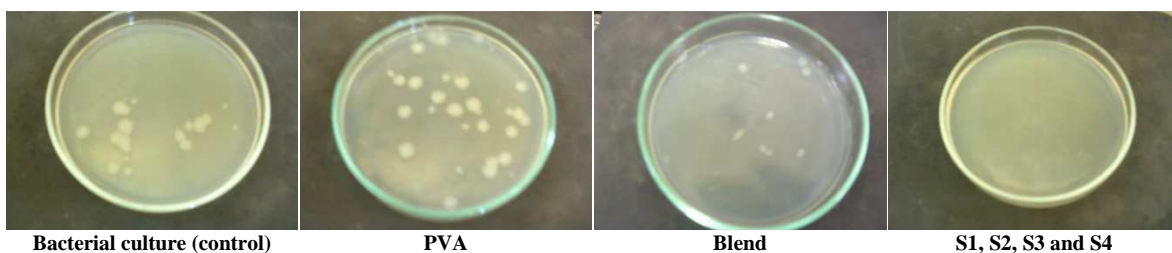


Fig.7: *Staphylococcus aureus* colony forming units of untreated (control, culture medium) and different films (PVA, blend, S1, S2, S3 and S4 at 0.2g/25ml culture)

Table (2): The antimicrobial activity of different samples using agar diffusion disk method

Sample	Clear zone (mm)			
	<i>Staphylococcus aureus</i>	<i>E. coli</i>	<i>Candida albicans</i>	<i>Aspergillus niger</i>
PVA	-	-	-	-
S0 (PVA/CS)	-	-	-	-
S1(PVA/CS/Ag0.1)	21	20	19	25
S2(PVA/CS/Ag0.2)	22	21	21	35
S3(PVA/CS/Ag0.4)	23	23	23	40
S4(PVA/CS/Ag0.8)	25	23	23	45

3.6. Determination of antibacterial activity by measuring the absorbance and CFU

The results represented in Table 3 and Fig. 7 exhibit the antimicrobial activity against *S. aureus* by measuring the CFU (colony forming units) and the reduction of UV absorption for the control sample (pure *S. aureus* culture) and the cultures containing 0.2 g/25 ml in Erlenmeyer flasks (vol. 100 ml). Figure 8 shows the growth in the flasks of control, PVA and the samples (S1, S2, S3 and S4) at concentrations of 0.2 g/25 ml. The results shows that a reduction in the bacterial growth has been found in the samples S1, S2, S3 and S4 and nothing happen with the pure PVA and PVA/CS blend.

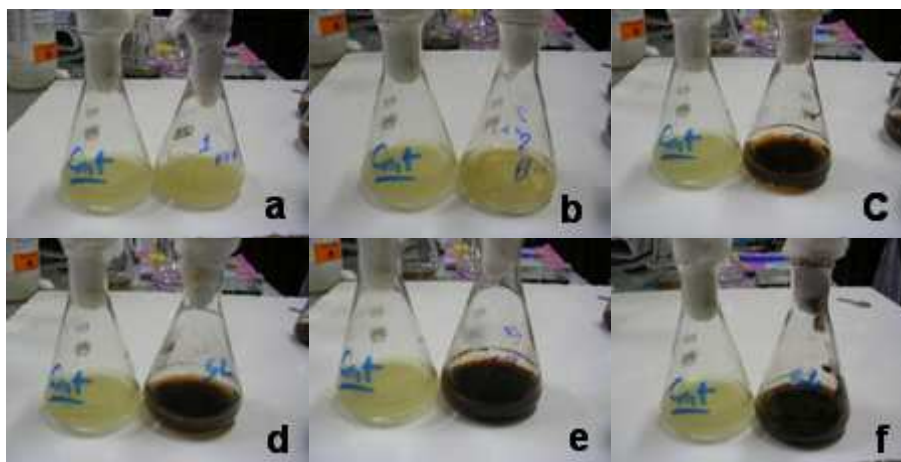


Fig.8: The growth density of *Staphylococcus aureus* culture (control), PVA, blend, S1, S2, S3 and S4 samples (a-f) (control on the left and the sample on the right)

Table (3): Antibacterial activity of treated and untreated samples in comparison to control (*Staphylococcus aureus* culture) using CFU and UV reduction techniques

Sample	Absorbance at 660 nm	Number of CFU ($10^7/\text{ml}$)	Reduction in CFU (%)
Bacterial culture	1.602	2.50	0.00
PVA	1.659	2.70	0.00
S0 (PVA/CS)	0.072	0.00	100
S1(PVA/CS/Ag0.1)	0.047	0.0	100
S2(PVA/CS/Ag0.2)	0.088	0.00	100
S3(PVA/CS/Ag0.4)	0.240	0.00	100
S4(PVA/CS/Ag0.8)	0.102	0.00	100

CONCLUSION

Equal mass pristine polymer blends of CS/PVA samples and the same samples doped with different concentrations of AgNP were prepared and studied. Examination of prepared nano-composites by XRD indicates the presence of a broad band at about 18.6° which is assigned to PVA/CS blend and the appearance of two new peaks at 32° and 46° were assigned to the face centered cubic (fcc) structure of the embedded Ag nano-particles, corresponding to hkl (111) and (200), respectively. FT-IR spectra show maintenance of the basic vibrational band corresponding to CS and PVA. UV/vis. absorption spectral data indicate the presence of absorption band at about 246 nm due attributed to $\pi \rightarrow \pi^*$ transitions, which is suggested to be from unsaturated bonds C=O and/or C=C. These results indicate the complexation between all the components and the change in crystallinity with the change in the AgNPs concentration. The nanocomposite samples show better film properties than that of pristine polymer blend without silver nanoparticles. It is obvious that nanocomposite samples exhibit an antibacterial effect against gram-positive and negative bacteria.

REFERENCES

- [1] S. Bajpai, Y.M. Mohan, M. Bajpai, R. Tankhiwale, V. Thomas, *Journal of nanoscience and nanotechnology*, **7** (2007) 2994-3010.
- [2] W.K. Son, J.H. Youk, W.H. Park, *Carbohydrate Polymers*, **65** (2006) 430-434.
- [3] A.M. Abdelgawad, S.M. Hudson, O.J. Rojas, *Carbohydrate polymers*, **100** (2014) 166-178.
- [4] G. Crini, P.-M. Badot, *Progress in polymer science*, **33** (2008) 399-447.
- [5] T.S. Trung, W.W. Thein-Han, N.T. Qui, C.-H. Ng, W.F. Stevens, *Bioresource technology*, **97** (2006) 659-663.
- [6] K. Kurita, K. Tomita, T. Tada, S.-I. Nishimura, S. Ishii, *Polymer Bulletin*, **30** (1993) 429-433.

- [7] D. Ting, Y. Shen, *Dyeing Finishing*, **14** (2005) 12-14.
- [8] M. Zeng, Z. Fang, C. Xu, *Journal of Applied Polymer Science*, **91** (2004) 2840-2847.
- [9] H.-S. Kim, K.-H. Lee, S.-G. Kim, *Aerosol science and technology*, **40** (2006) 536-544.
- [10] S. Liu, J. He, J. Xue, W. Ding, *Journal of Nanoparticle Research*, **11** (2009) 553-560.
- [11] S. Tripathi, G. Mehrotra, P. Dutta, *International journal of biological macromolecules*, **45** (2009) 372-376.
- [12] T.V. Duncan, *Journal of colloid and interface science*, **363** (2011) 1-24.
- [13] R. Jung, Y. Kim, H.-S. Kim, H.-J. Jin, *Journal of Biomaterials Science, Polymer Edition*, **20** (2009) 311-324.
- [14] M. Rai, A. Yadav, A. Gade, *Biotechnology advances*, **27** (2009) 76-83.
- [15] M. Catauro, M. Raucchi, F. De Gaetano, A. Marotta, *Journal of Materials Science: Materials in Medicine*, **15** (2004) 831-837.
- [16] J.H. Crabtree, R.J. Burchette, R.A. Siddiqi, I.T. Huen, L.L. Hadnott, A. Fishman, *Peritoneal Dialysis International*, **23** (2003) 368-374.
- [17] D.C. Tien, K.-H. Tseng, C.-Y. Liao, T.-T. Tsung, *Journal of Alloys and Compounds*, **473** (2009) 298-302.
- [18] J.S. Kim, E. Kuk, K.N. Yu, J.-H. Kim, S.J. Park, H.J. Lee, S.H. Kim, Y.K. Park, Y.H. Park, C.-Y. Hwang, *Nanomedicine: Nanotechnology, Biology and Medicine*, **3** (2007) 95-101.
- [19] R. Kumar, H. Münstedt, *Polymer international*, **54** (2005) 1180-1186.
- [20] J.J. Castellano, S.M. Shafii, F. Ko, G. Donate, T.E. Wright, R.J. Mannari, W.G. Payne, D.J. Smith, M.C. Robson, *International Wound Journal*, **4** (2007) 114-122.
- [21] M. Mishra, H. Kumar, K. Tripathi, *Dig J Nanomater Bios*, **3** (2008) 49-54.
- [22] M.I. Sriram, S.B.M. Kanth, K. Kalishwaralal, S. Gurunathan, *International journal of nanomedicine*, **5** (2010) 753.
- [23] R. Vaidyanathan, K. Kalishwaralal, S. Gopalram, S. Gurunathan, *RETRACTED: Nanosilver—The burgeoning therapeutic molecule and its green synthesis, Biotechnology Advances*, **27** (2009) 924-937.
- [24] P. Sanpui, A. Chattopadhyay, S.S. Ghosh, *ACS applied materials & interfaces*, **3** (2011) 218-228.
- [25] P. Sanpui, A. Murugadoss, P. Prasad, S.S. Ghosh, A. Chattopadhyay, *International journal of food microbiology*, **124** (2008) 142-146.
- [26] A.D. Tiwari, A.K. Mishra, S.B. Mishra, A.T. Kuvarega, B.B. Mamba, *Carbohydrate polymers*, **92** (2013) 1402-1407.
- [27] J. Jain, S. Arora, J.M. Rajwade, P. Omray, S. Khandelwal, K.M. Paknikar, *Molecular Pharmaceutics*, **6** (2009) 1388-1401.
- [28] C.E. Hoppe, M. Lazzari, I. Pardiñas-Blanco, M.A. López-Quintela, *Langmuir*, **22** (2006) 7027-7034.
- [29] C. Collins, P. Lyne, J. Grange, *Counting methods*, Collins' and Lyne's Microbiological Methods, 7th edn. Oxford, London: Butterworth Heinemann, (1995) 149-162.
- [30] M.S. Abdel-Aziz, A. Hezma, *Polymer-Plastics Technology and Engineering*, **52** (2013) 1503-1509.
- [31] D.S. Arora, J. Kaur, *International Journal of Antimicrobial Agents*, **12** (1999) 257-262.
- [32] D. Gupta, S.K. Khare, A. Laha, *Coloration Technology*, **120** (2004) 167-171.
- [33] R.J. Samuels, *Journal of Polymer Science: Polymer Physics Edition*, **19** (1981) 1081-1105.
- [34] I. Ahmed, A. Idris, M.Y. Noordin, R. Rajput, *Industrial & Engineering Chemistry Research*, **50** (2011) 2272-2283.
- [35] A. Abdelghany, E. Abdelrazek, D. Rashad, *Spectrochimica Acta Part A: Molecular and Biomolecular Spectroscopy*, **130** (2014) 302-308.